Preliminary studies of the impact on temperature of a high-power laser on-board a 6U CubeSat

Edemar Morsch Filho, Rodrigo Santiago, Mateus M. B. Costa, Kleber V. Paiva, Talita S. Possamai, et al.

Edemar Morsch Filho, Rodrigo Santiago, Mateus M. B. Costa, Kleber V. Paiva, Talita S. Possamai, Renato Oba, Vicente P. Nicolau, Gary B. Hughes, "Preliminary studies of the impact on temperature of a high-power laser on-board a 6U CubeSat," Proc. SPIE 10769, CubeSats and NanoSats for Remote Sensing II, 107690U (18 September 2018); doi: 10.1117/12.2319766

SPIE.

Event: SPIE Optical Engineering + Applications, 2018, San Diego, California, United States

Preliminary studies of the impact on temperature of a high-power laser on-board a 6U Cubesat

Edemar Morsch Filho*[a], Rodrigo Santiago[a], Mateus M. B. Costa[a], Kleber V. Paiva[a], Talita S. Possamai[a], Renato Oba[a], Vicente P. Nicolau[b] and Gary B. Hughes[c]
[a] Thermal Fluid Flow Group – T2F, Department of Mobility Engineering, Federal University of Santa Catarina, Joinville, SC, Brazil; [b] Department of Mechanical Engineering, Federal University of Santa Catarina, Florianópolis, SC, Brazil; [c] California Polytechnic State University, Statistics Department, 25-107G, 1 Grand Avenue, San Luis Obispo, CA 93407-0405

ABSTRACT

Numerical simulation of heat transfer on a 6U CubeSat is performed. The spacecraft's primary mission is a space environment demonstration of a NASA Innovative Advanced Concepts (NIAC) project for the measurement of asteroid composition using a high-power laser. The laser works on cycles of 10 seconds on and 10 minutes off. Approximately 200 W is dissipated as heat when the laser is on. Attitude control mechanisms maintain the laser pointing towards the target, and also keep the spacecraft between the sun and the target. Simulations are performed using ANSYS CFX; boundary conditions are inserted as User Defined Functions. Mechanical design includes a network of heat pipes and passive radiative surfaces for heat distribution and expulsion. Four cases are addressed, all with orbit inclination of 90° and 650 km altitude. Two simulations have ascending node equal to 90°, named as hot cases. The remaining two cases have ascending node equal to 0, referred to as cold cases. For the hot case and laser turned off, the maximum and minimum temperatures obtained are 344 K and 282 K, respectively. Temperatures of 352 K and 287 K are found for this same orbit, but with the laser on. For the cold case and laser always off, extreme onboard temperatures are 334 K and 263 K, and with laser working, extremes are 342 K and 268 K. In all simulations the highest temperatures are on surfaces facing the sun while the lowest are on the opposite side. For the operating mode of the laser, its results for range of temperature on orbit are outside the suggested from manufacturer.

Keywords: nanosatellite, laser, numerical analyses, thermal control.

1. INTRODUCTION

1.1 The concept of NIAC

NASA Innovative Advanced Concepts (NIAC) is a program which gives opportunities to grow visionary ideas that may someday change the future of space missions, either with new brand aerospace technologies and concepts or improvements in well-established technologies[1]. The mission in this paper is part of NIAC and is called molecular composition analysis of distant targets. The goal of the mission is to probe the molecular composition of some solar system targets, like asteroids, planets and even others further away targets.

To prove the feasibility of the mission, a 6U CubeSat (mother ship) that carries a laser and another spacecraft will be launched in a circular Low Earth Orbit (LEO). The laser will be used for a Remote Laser Evaporative Molecular Absorption (R-LEMA) spectroscopy which its primary task is to measure composition of diverse substances. The laser will point towards the target, as for example another CubeSat, and heats up its surface, evaporating the superficial material of the object. A molecular cloud (plume) will form and then be analyzed by the infrared absorption spectroscopy[2]. In the present paper, the thermal field of the 6U CubeSat in LEO is simulated.

* edemar@labcet.ufsc.br; phone 55 48 3721 9390

CubeSats and NanoSats for Remote Sensing II, edited by Thomas S. Pagano, Charles D. Norton, Proc. of SPIE Vol. 10769, 107690U · © 2018 SPIE
CCC code: 0277-786X/18/$18 · doi: 10.1117/12.2319766

1.2 Structure and components

The main components on board of NIAC are listed on Table 1 together with their respective power consume and operational limits of temperature. It is observed that the laser and battery have particular scenarios of operation in terms of temperature. In addition to that, the energy required to proper function of the laser is much greater than the other's equipment. The laser that will be used in the mission is an element e18 Fiber Coupled Diode Laser®. This equipment offers up to 220 W of output power from a 200 μm fiber and wavelengths of 793, 808, 885, 915, 940, 969, 976 nm under a stabilized spectrum over temperature and current. The laser operates in cycles with approximately 10 s on followed by 10 minutes off. During its operational mode, around 200 W is converted into heat and dissipates through the structure by conduction and radiation.

Table 1. Operational parameters of main parts of the CubeSat.

Part		Consume [W]	Temperature range [K]
Laser[3]	Operational	512	293 to 308
Laser	Stand-by	0	253 to 343
Spectrometer[4]		1.40	253 to 313
Reaction wheel[5]		0.18	263 to 343
Micro thruster[6]		2.00	253 to 343
ADCS control[7]		1.00	263 to 333
Antenna[8]		4.00	253 to 333
Antenna deployment mechanism[9]		2.00	253 to 333
Attitude sensor[10]		0.36	263 to 343
Computer[11]		0.55	248 to 338
Battery[12]	Charge	0.02	273 to 318
Battery	Discharge	0.02	253 to 333
Structure[13]		0	233 to 353
Photovoltaic panel[14]		0	233 to 358

Preliminary simulations of heat transfer on this satellite are conducted to get insight about the thermal environment that it will face on orbit. The objective is to get useful results about its behavior and then guide the next steps for the development of the CubeSat. To address these tasks, Computational Fluid Dynamics (CFD) are used to simulate its transient temperature field for the extreme cases with and without eclipse of the Earth and in both configuration of laser operational and stand-by.

2. LITERATURE REVIEW

Diverse methods to solve the problem of heat transfer on satellites are available in the literature, differing on complexity, resolution, precision and computational cost, for both commercial and non-commercial software. The general idea behind these methods is to divide a volume into smaller parts, solve the equations in these sub-domains and then group the results to compose the solution of the whole domain. For problems of fluid mechanics, they are based on partial differential equations (PDE) and referred to the laws of conservations, which require boundary conditions to be solved. The most commons are the Lumped Parameter Method (LPM), Finite Difference Method (FDM), Finite Element Method (FEM) and Finite Volume Method (FVM).

In LPM, a network method is used to represent the system. The spatial domain is divided into nodes and each point represents one component of the Cubesat. The FDM differentiates from the LPM by discretizing spatially the physical domain, where the equation is approximated by numerical finite differences based on Taylor's series approach and applied in the nodes. On the other hand, FEM applies a more complex numerical discretization than FDM and allows higher degree of detailing of the phenomena, but the drawback is computational cost. In theory, FEM can predict the solution in every point of domain because it uses functions to interpolate the results on the elements between the nodes. FVM solves the problem in cells instead on nodes and integrates the PDEs over its boundaries. Its integral on volumes results in a conservative method by nature, where the balances must necessarily close.

The influence of altitude, radiator area and material properties of satellite TUU-SAT1 was assessed through LPM formulation[15]. The FEM method was applied to solve the temperature field of the microsatellite HAMSAT equipped with passive thermal control. Its performance on orbit matches with the predictions obtained with the software IDEAS-

TMG[16]. Numerical results of nanosatellite OUFTI-1 were confronted with Matlab/Simulink and ESATAN/ESARAD software and results indicated inappropriate temperature field for the batteries. A heating system was designed and showed potential to keep the batteries within the range of acceptable temperature[17]. Using FEM, the PiCPoT nanosatellite was thermally simulated and the results were used to refine the project and attend the requirements of temperature. Appropriate range of temperature was obtained by passive control, basically coatings and thermal tapes, but heaters were designed for the batteries to prevent too cold scenarios[18].

The temperature field of picosatellite YamSat was solved with the commercial software TRASYS and SINDA[19]. The focus of the authors was the impact of superficial and material properties of the satellite and passive thermal control methods were appropriate to keep all the subsystems working properly. FloripaSat-1 was simulated for diverse orbit inclination under FVM formulation and the authors concluded that the eclipse and solar radiation were two parameters that played important role in the temperature field of the satellite[20]. Influence of orbit inclination, altitude and spin rate on the thermal analysis of CubeSats were already conducted on SINDA and Thermal Desktop, using a formulation LPM, and the results indicated homogenization of temperature as the spin increases[21]. The CubeSat Turksat 3U was simulated in ThermXL and authors found temperature fields within the hot temperatures but below the minimum temperatures, concluding that heaters would be a simple solution to end this problem[22, 23].

Observing the general aspects of these researches, they are focused on the extreme temperatures for hot and cold cases, addressed by combination of attitude and energy harvesting. In general, small satellite face problem related to cold temperatures, however none of them had massive generation of heat by modules as the present study, due to the laser system.

3. METHODOLOGY

3.1 Orbit and attitude

As the CubeSat for project NIAC is an ongoing project, it is important to mention that some of the following considerations are not representative of the current status of development of CubeSat NIAC. Few of the information used to set the problem, especially about parameters of the laser, were not available when the simulations ran and estimations were made to select representative values for this study. Nevertheless, the results and conclusions stand acceptable to orientate this project, which is in the early stage and whose specific solutions of engineering are not yet defined.

The simulations are valid for a CubeSat 6U at the altitude of 650 km, circular orbit, inclination of 90º and zero spin around its own axes. Two extreme scenarios are tested, one without eclipse of the Earth (hot case) and one with the eclipse of the Earth (cold case). For each situation there are two different configurations, one with the laser operating for 10 seconds and turning off every 10 minutes and other with the laser always off. For all the cases, the satellite always keeps the side +Y towards the Sun, as shown in Figure 1.

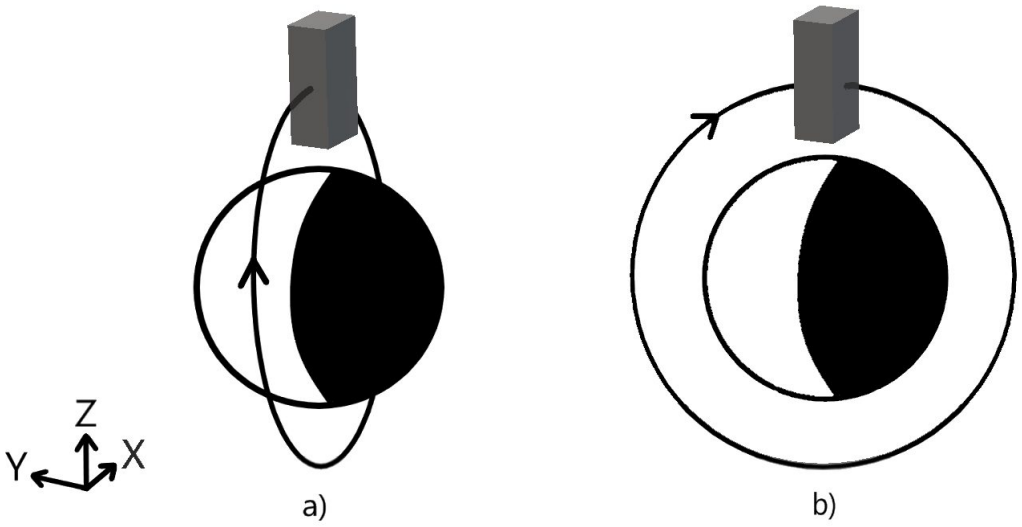

Figure 1. Orbit and attitude. a) Without eclipse; b) With eclipse.

3.2 Thermal analysis

The simulations performed in this study have the idealization of gray, diffuse and opaque surfaces, resulting that the emissivity and absorptivity are equal for any range of the radiation spectrum. The energy absorbed by radiation is transferred throughout the structure of the satellite by conduction and a portion of it is emitted back to outer space by radiative processes. Direct sunlight, albedo and infrared radiation of planets are the external sources of energy over the satellite[24, 25]. The satellite only receives solar radiation when it is not under the eclipse. Albedo exists when it is on the illuminated side of the Earth, whose peak coincides with the equatorial plane and the infrared radiation happens for the entire orbit. For the case without eclipse, the satellite surrounds the Earth exactly at the border between night and day, so only solar and infrared radiations reach the satellite while albedo is null.

The general energy equation of conservation is given by Equation 1.

$$mc_p \frac{dT}{dt} = Q_{r,net} - Q_{cond} + Q'''\forall \tag{1}$$

where m is the mass of the volume, c_p the specific heat at constant pressure, T the temperature, t the time, $Q_{r,net}$ the net radiative heat rate for that volume, Q_{cond} the net conductive heat rate between adjacent volumes and Q''' the volumetric source of heat generation of internal components multiplied by the volume $\forall$. Effects of convection are not considered in this work.

The net radiative heat rate ($Q_{r,net}$) accounts for all the ways that the satellite exchanges heat by radiative processes. It is the sum of direct absorbed radiation from Sun (Q_{sun}), absorbed radiation from reflectance of the Earth (Q_{alb}), absorbed infrared radiation emitted from Earth (Q_{IR}) and emitted radiation from CubeSat to outer space ($Q_{sat\rightarrow spa}$), as shown in Equation 2.

$$Q_{r,net} = Q_{sun} + Q_{alb} + Q_{IR} - Q_{sat\rightarrow spa} \tag{2}$$

In this work, the inner sides of the satellite are adiabatic ($Q_{r,net} = 0$). This idealization avoids the formulation of successive heat exchanges among surfaces inside the CubeSat and reduces the computational cost. As consequence, it is expected that the value of temperature will be overestimated and underestimated in a few degrees for hot and cold parts of the satellite, respectively.

Radiation from Sun is the most significant heat source for satellites in LEO. The constant value adopted here is $Q_s'' = 1360$ W/m² for the solar flux radiation and it is assumed that the solar rays are parallel[24, 25]. Absorbed solar radiation is modeled by Equation 3.

$$Q_{sun_p} = \alpha_s Q_s'' A_p F_{sun\rightarrow sat,p} \Psi \tag{3}$$

where α_s is the satellite surface absorptivity in the Sun's emission spectrum, A_p is the exposed area to the solar flux, $F_{sun\rightarrow sat,p}$ is the view factor of the surface p in relation to the Sun and parameter Ψ is a step function created to become zero when the satellite is under the shadow of the Earth[26]. The view factor of surface p towards the Sun is calculated by Equation 4, which depends of the surface orientation ($\overrightarrow{n_p}$) and the position of the Sun ($\vec{S}$).

$$F_{sun\rightarrow sat,p} = \begin{cases} |\overrightarrow{n_p}.\vec{S}|, & \overrightarrow{n_p}.\vec{S} < 0 \\ 0, & \overrightarrow{n_p}.\vec{S} \geq 0 \end{cases} \tag{4}$$

The absorbed albedo radiation is defined by Equation 5.

$$Q_{alb,p} = a\alpha_s Q_s'' A_p F_{earth\rightarrow sat,p} f \tag{5}$$

where a is the albedo coefficient representing the reflected solar radiation from surface of the Earth and $F_{earth\rightarrow sat,p}$ is the view factor between the surface p and Earth. The last term f models albedo as a specular source. Its peak coincides with latitude 0 and Sun in zenith, calculated in Equation 6. $\overrightarrow{R_s}$ is the position on orbit of the satellite.

$$f = \begin{cases} -\dfrac{\overrightarrow{R_s}.\vec{S}}{|\overrightarrow{R_s}|}, & -\overrightarrow{R_s}.\vec{S} > 0 \\ 0, & -\overrightarrow{R_s}.\vec{S} \leq 0 \end{cases} \tag{6}$$

The value of coefficient a changes accordingly to characteristics of surfaces of the Earth as soil, type of vegetation, presence of clouds and oceans, so an intermediary value of 30 % is applied[24]. To calculate $F_{earth \rightarrow sat,p}$ it is assumed that Earth is a spherical emitter whose dimension is much bigger than the satellite, and the view factor is function of the distance between the satellite and the Earth, as well the angle between these surfaces[26].

The last external source of heat presented on the satellite is the absorbed infrared radiation from Earth, written in Equation 7.

$$Q_{IR,p} = \alpha_{IR} Q''_e A_p F_{earth \rightarrow sat,p} \quad (7)$$

where α_{IR} is the surface absorptivity in the infrared spectrum and the infrared radiation heat flux emitted by Earth (Q''_e) is constant and equal to 237 W/m² [24, 25].

The satellite emits radiation to outer space according to Equation 8.

$$Q_{sat \rightarrow spa,p} = \varepsilon_{IR} A_p \sigma \left(T^4_{sat,p} - T^4_{spa} \right) \quad (8)$$

where ε_{IR} is the emissivity of the surface in the infrared spectrum, σ the Stefan-Boltzmann constant (5.67×10^{-8} W/m^{2}K^4), $T_{sat,p}$ is the temperature on the surface p and T_{spa} is the temperature of space, here considered 2,7 K.

Heat conduction through the domain (Q_{cond}) is given by the integral form of the Fourier Law over the surface of a differential volume, where k is the thermal conductivity of the material, ∇T the gradient of temperature and $\vec{A}$ the surface of the volume, as shown in Equation 9.

$$Q_{cond} = \oint k \nabla T . d\vec{A} \quad (9)$$

Besides radiation heat exchange processes, the electronic devices may generate heat. However, in this work they are neglected due to their low power, except for the laser, which dissipates 200 W of heat equally distributed over its volume.

3.3 Numeric domain and convergence criteria

As shown in Table 1, laser is a critical component in the satellite and for this reason, the focus is on its behavior and heat diffusivity throughout the structure. Figure 2 shows the current engineering model (a) and the simplified numeric domain (b). These adaptations keep the computational cost low and facilitate the construction of the mesh and set up of the problem. Structure (blue), solar panels (gray) and laser (red) are in the model for the simulations. A major difference between both models that readers should be aware is on the laser geometry, shaped box for the current status and cylindrical for the simulations. It happens because there was no information about this component when the analyses were conducted.

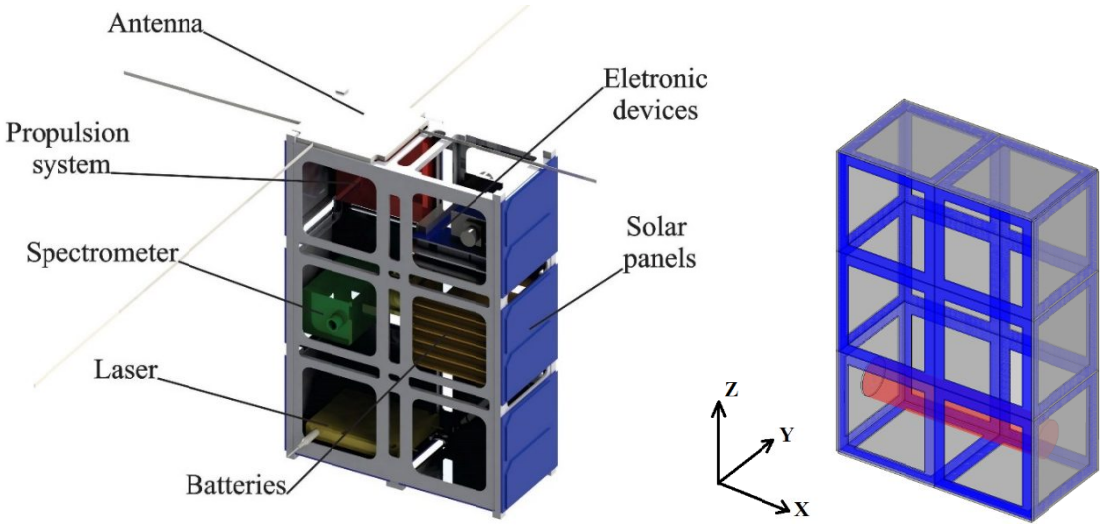

Figure 2. a) Current engineering model; b) Numeric domain for thermal simulations.

The external dimensions of the CubeSat are 300 x 100 x 200 mm, as the standard CubeSat 6U[27]. Each side of the satellite is named accordingly to its frame of reference, namely –X, +X, -Y, +Y, -Z and +Z. The normal vector on side +Y is parallel to solar rays and faces the Sun. As the satellite does not spin around its axes, this side always points towards the Sun, while the opposite (-Y) is every tine under the shadow and for this reason there are not solar panels in the +Y side.

A total of 4 unstructured hexahedra meshes were created on the software Ansys ICEM for the solar panels, laser and structure, as observed on Figure 3. Due to symmetry, the top left and right parts of the structure, as well the bottom left and right parts (Figure 2. a) have identical grids, but mirrored. The middle left and right part of the structure (Figure 2. b) are built with two equal meshes, also opposed to each other. All the solar panels (Figure 2. c) replicate the same mesh and the laser is constructed as a singular one (Figure 2. d). The grid has a total of 185840 nodes and 136735 volumes.

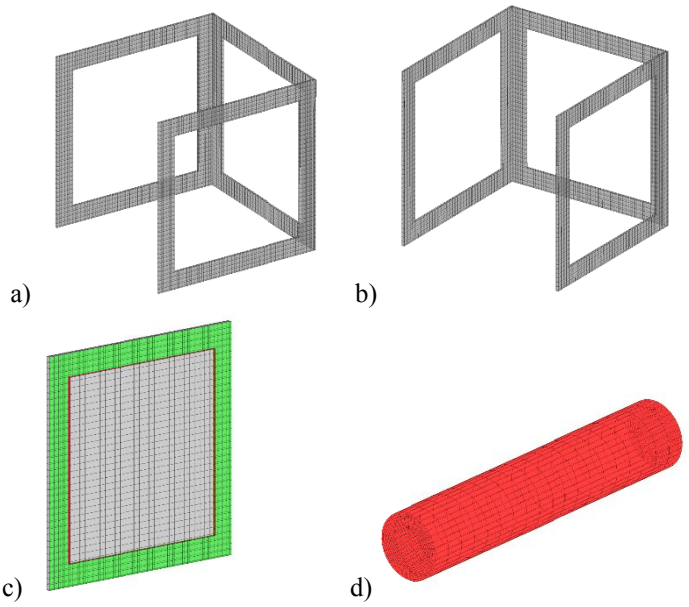

Figure 3. Meshes of the numeric domain.

The thermodynamic properties of the materials used in the satellite are summarized in Table 2.

Table 2. Material property[28].

Component	Material	ρ [kg/m^3]	k [W/mK]	ε [-]	c_p[kJ/kgK]
Structure	Aluminum	2810	130	0.4	960
Board	Fiberglass	2400	1.03	0.3	800
Solar Panel	Fiberglass	2810	1.03	0.3	800
Battery	Polyethylene	9200	0.4	0.3	1250
Laser	Copper	8933	401	0.3	385

As the laser was not defined until the end of this work, a regular material was selected to represent it. The choice for copper was because its good properties for dissipation of heat, which can be seen as an extreme good scenario.

The transient thermal simulations are performed in the commercial software Ansys CFX, which bases on FVM to solve the conservative energy equation. The convergence criterion is an error in the balance below 1% and periodic temperature fields for the points monitored. This last condition is valid for cyclic boundary conditions, as the case herein.

4. RESULTS

This section shows the results of temperature on the external surfaces of the satellite. One point for each side and laser are provided for a full converged orbit. Figure 4 shows results of temperature for the orbit without eclipse and laser always off. While extreme temperatures on solar panels are around 282 K and 344 K, laser has an intermediary value of 300 K. The small variation on the fields come from the fact that the satellite does not spin and the same side (+Y) faces

the Sun during the entire orbit. The oscillations, mainly on the other sides, are due the exposition to infrared radiation, which does not happen constantly because of changes in the view factor as the satellite rounds the Earth. As expected, the sides opposite to the Sun are the coldest because they only receive infrared radiation and heat through the structure.

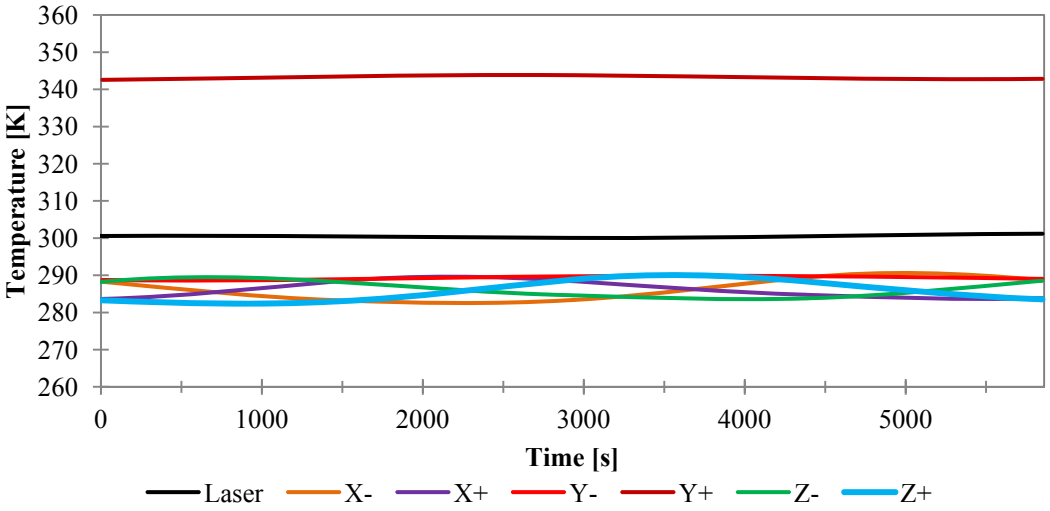

Figure 4. Hot case: Eclipse off and laser off.

Figure 5 is valid for the condition without eclipse but with the laser operating. The generation and dissipation of heat by the laser is remarkable on its temperature data. The peaks occurring during the operation for 10 seconds and its cool down for 10 minutes impact on the thermal field of the entire satellite. In general, all the points measured on the external surfaces raise up their values around 10 K, while on the laser it is roughly 15 K. The extreme temperature of 352 K on side Y+ is 65 K greater than the minimum registered on Z+. The operational cycle is fast and powerful enough to keep the satellite warmer than previous case even when the laser is off. The diffusion of heat through the structure is quick due good properties of conductivity of the aluminum. The variation of temperature in the laser around 5 K is small, but it results from the thermodynamic properties set to it and valid for a solid cylinder of copper. For this condition, the laser has an intermediary temperature when compared to the other points.

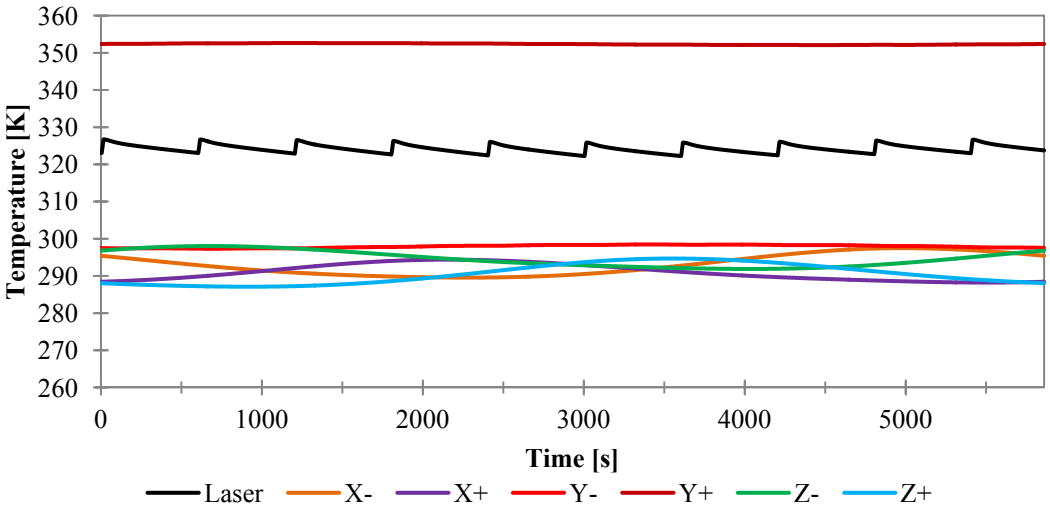

Figure 5. Hot case: Eclipse off and laser on.

Results for the orbit with eclipse and laser off are available on Figure 6. Drastic changes occur in the thermal field, especially because the shadow of the Earth observed in the center of the graph between 1700 s and 4000 s. The absence of solar radiation drops the temperature, mainly on the side Y+ previously exposed to the Sun. The evidence of transient

values is more evident, around 20 K for sides that never experience the Sun and 60 K for the opposite (Y+). The laser also faces a gradient of 10 K and in general its temperature is closer to the vicinity. The maximum temperature on the external sides is 334 K and the minimum is 263 K, however they do not occur at the same instant. The maximum of 59 K and minimum of 9 K happen in the beginning and end of the shadow, respectively. Probably because the laser is enclosed by the satellite and its thermal inertia, near the end of the shadow it is the hottest part measured.

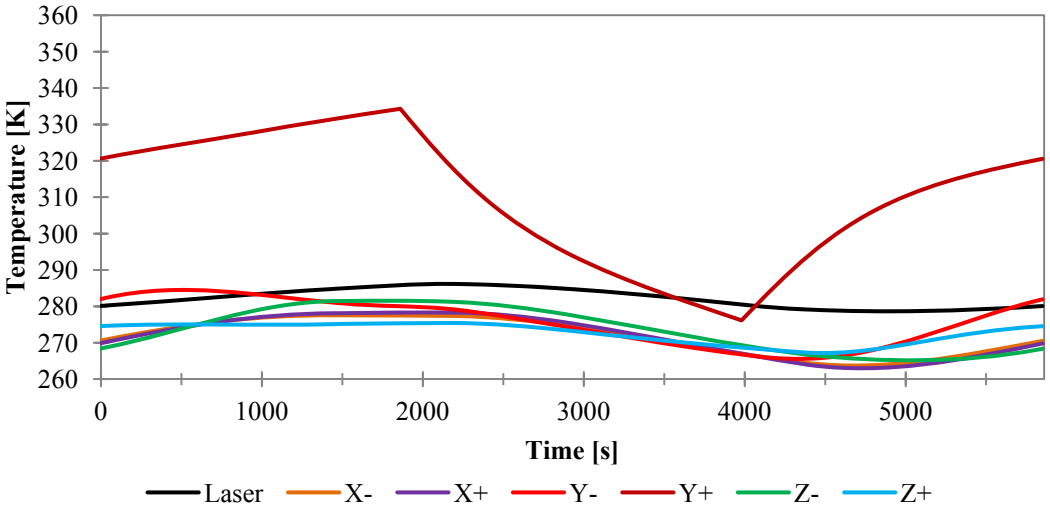

Figure 6. Cold case: Eclipse on and laser off.

Figure 7 presents the results for the case of orbit with eclipse and configuration of laser turned on, according to its operational cycle. As observed on Figure 5, the values increase for this condition, however the shadow is still able to reduce the overall temperatures. Augmentation not greater than 5 K are observed in the laser during its cycle of operation, but now its extreme temperature is over 310 K while the minimum is bigger than 300 K. The greatest difference of temperature is 63 K at the beginning of the shadow and 18 K at the end. For this condition, the laser is warmer than other parts of the satellite during half of the time under the shadow and assumes intermediary values for the remaining time.

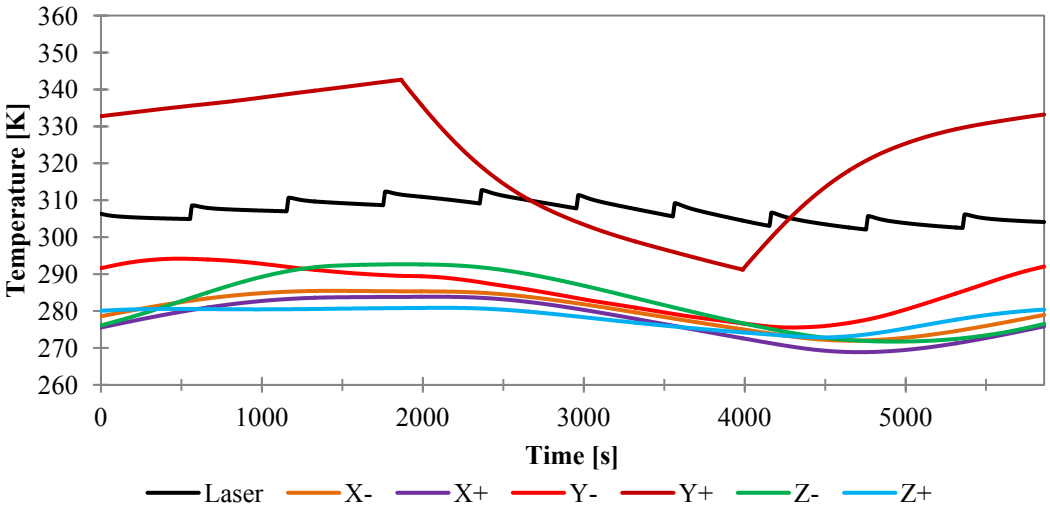

Figure 7. Cold case: Eclipse on and laser on.

The temperatures on the laser for each condition are plotted in Figure 8, as well its temperature limits for the operational and stand-by mode. For the condition in which laser is not working (red and blue dot lines), in both cases with and without eclipse, its temperature ranges on orbit are appropriate when compared to the recommended values of the

manufacturer (see Table 1). However, when the laser is operating (red and blue lines), the satellite structure itself fails to provide appropriate thermal dissipation. During the whole orbit, laser temperature is outside of the recommended range for the case without eclipse, while with eclipse and laser operating there are periods where the temperatures are above the safety condition. In both cases, the satellites fails due overheating of the laser. Due to the hypotheses assumed in the modeling, particularly related to laser material, which is more conductive than the real equipment, laser thermal dissipation inspires attention. Further analysis and solution for thermal control will be required.

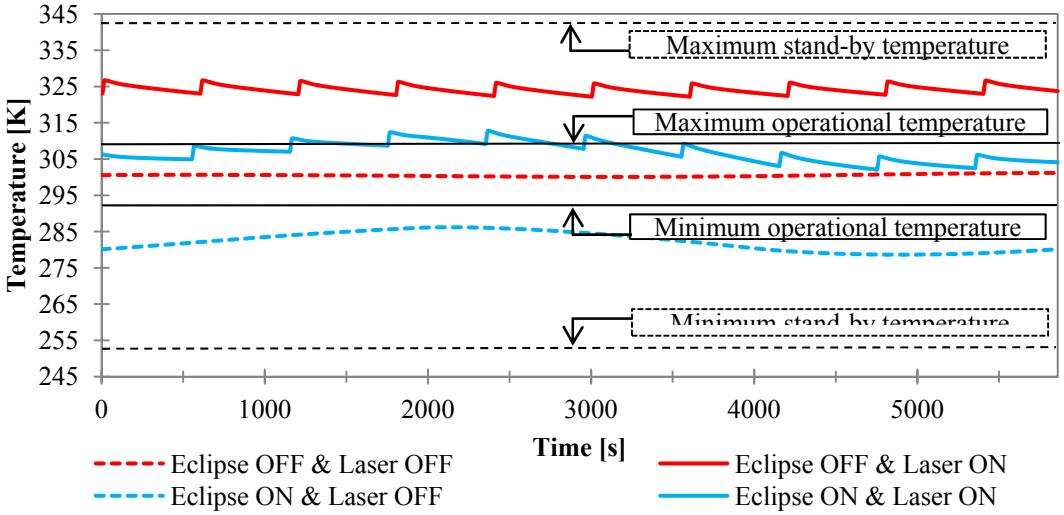

Figure 8. Temperature on the laser for each scenario.

5. CONCLUSIONS

A preliminary study about the thermal behavior of the 6U CubeSat under NIAC project was conducted through numerical simulations in CFD for two conditions of eclipse and laser operation. A simplified model of the satellite structure and laser was implemented to investigate the initial thermal conditions cubesat may be exposed in LEO. The attitude of one side facing the Sun resulted in high temperature gradients, with one surface always hotter than remaining. Concern must be taken about the excessive heat generation in the laser system that overheats and jeopardizes the mission. Further studies are required to understand how harmful it is and what technology could mitigate this problem. Passive thermal controls devices could be employed since there are colder spots in the satellite for every instant of orbit.

For future studies, it is suggested to update the numeric model with more precise information about the laser, especially about its geometry, thermodynamic properties, power dissipation and operational cycle. The temperature over the batteries should also be simulated to identify hazardous conditions for their proper operation and then propose solutions to avoid failure in the power supply and in the overall mission of CubeSat NIAC.

ACKNOWLEDGEMENTS

The present work was realized with the support of CNPQ, National Council of Scientific and Technological Development – Brazil, for providing the scholarship under grant number 141276/2018-5.

REFERENCES

[1] NASA, “NIAC Overview”, URL: https://www.nasa.gov/content/niac-overview [retrieved 28 June 2018]
[2] Hughes, G, “Remote Laser Evaporative Molecular Absorption Spectroscopy Sensor System”, 2017. URL:https://www.nasa.gov/directorates/spacetech/niac/2017_Phase_I_Phase_II/Remote_Laser_Evaporative_Molecular_Absorption_Spectroscopy_Sensor_System [retrieved 24 June 2018]
[3] nLIGHT, “element® e18 Fiber Coupled Diode Laser”, URL: http://www.nlight.net/products/diode-lasers/120-element-e18-Fiber-Coupled-Diode-Laser [retrieved 25 June 2018]
[4] CubeSatShop, “Argus 1000 Infrared Spectrometer”, URL:

https://www.cubesatshop.com/product/argus-1000-infrared-spectrometer/ [retrieved 25 June 2018]
[5] CubeSatShop, “CubeWheel Medium”, URL: https://www.cubesatshop.com/product/cubewheel-medium/ [retrieved 25 June 2018]
[6] CubeSatShop, “Nanosatellite Micropropulsion System”, URL: https://www.cubesatshop.com/product/nanosatellite-micropropulsion-system/ [retrieved 28 June 2018]
[7] CubeSatShop, “Cube ADCS”, URL: https://www.cubesatshop.com/product/cube-adcs [retrieved 25 June 2018]
[8] ISIS – Innovative Solutions In Space, “ISIS VHF uplink/UHF downlink Full Duplex Transceiver”, URL: https://www.isispace.nl/product/isis-uhf-downlink-vhf-uplink-full-duplex-transceiver/ [28 June 2018]
[9] CubeSatShop, “Deployable turnstile antenna system”, URL: https://www.cubesatshop.com/product/turnstile-antenna/ [retrieved 28 June 2018]
[10] CubeSatShop, “CubeSense”, URL: https://www.cubesatshop.com/product/cubesense/ [retrieved 28 June 2018]
[11] CubeSatShop, “ISIS On board computer”, URL: https://www.cubesatshop.com/product/isis-on-board-computer/ [retrieved 26 June 2018]
[12] GOMspace, “Standard battery module for small nanosatellites”, URL: https://gomspace.com/Shop/subsystems/batteries/nanopower-bp4.aspx [retrieved 26 June 2018]
[13] ISIS – Innovative Solutions In Space, “6-Unit CubeSat structure”, URL: https://www.isispace.nl/product/6-unit-cubesat-structure/ [retrieved 26 June 2018]
[14] GOMspace, “High efficiency modular solar panels for GomSpace 6U structure”, URL: https://gomspace.com/Shop/subsystems/solar-panels/msp-solar-panels.aspx [retrieved 26 June 2018]
[15] S.R. Lee, Z.C. Hong, K.T. Peng, L.S. Leu, “Analysis the Unsteady-State Temperature Distribution of Micro-Satellite Under Stabilization Effects”, Editor(s): Fei-Bin Hsiao, COSPAR Colloquia Series, Pergamon, Volume 10, 1999, Pages 324-332, ISSN 0964-2749, ISBN 9780444501967, doi.org/10.1016/S0964-2749(99)80041-9
[16] K. Badari Narayana, V. Venkata Reddy, “Thermal design and performance of HAMSAT”, Acta Astronautica, Volume 60, Issue 1, 2007, Pages 7-16, doi.org/10.1016/j.actaastro.2006.07.001
[17] Jacques, L., “Thermal design of the Oufti-1 nanosatellite”, Master Thesis, Applied Sciences Faculty, University of Liège, Liége, Belgium, 2009.
[18] S. Corpino, M. Caldera, F. Nichele, M. Masoero, N. Viola, “Thermal design and analysis of a nanosatellite in low earth orbit”, Acta Astronautica, Volume 115, 2015, Pages 247-261, ISSN 0094-5765, doi.org/10.1016/j.actaastro.2015.05.012.
[19] Hu, L., Chang, M. S., and Tsai, J. R., “Thermal control design and analysis for a picosatellite-Yamsat”, Transactions of the Aeronautical and Astronautical Society of the Republic of China, Vol. 35, No. 3, 2003, pp. 227-233.
[20] Morsch Filho, Edemar, “Simulação numérica da transferência de calor em um nanosatélite”, 76 pages. Final Project, Aerospace Engineering, Federal University of Santa Catarina, 2015.
[21] Farhani, F., and Anvari, A., ”Effects of some parameters on thermal control of a LEO satellite”, Journal of Space Science & Technology, Vol. 7, 2014, pp. 13-24.
[22] Bulut, Murat & Sözbir, Ömer & Sözbir, Nedim. (2017). “Thermal Control of Turksat 3U Nanosatellite”.
[23] Murat Bulut, Nedim Sozbir, “Analytical investigation of a nanosatellite panel surface temperatures for different altitudes and panel combinations”, Applied Thermal Engineering, Volume 75, 2015, Pages 1076-1083, ISSN 1359-4311, doi.org/10.1016/j.applthermaleng.2014.10.059
[24] Gilmore, D. G., “Spacecraft Thermal Control Handbook: Fundamental technologies”, 2nd ed., The Aerospace Corporation, California, 2002.
[25] Larson, Wiley J, and James R. Wertz. “Space Mission Analysis and Design”. Torrance, Calif: Microcosm, 1992. Print.
[26] Richmond, J. A., “Adaptive Thermal Modeling Architecture for Small Satellite Applications”, Master Thesis, Department of Aeronautics and Astronautics, Massachusetts Institute of Technology, Cambridge, US, 2010.
[27] Cal Poly, “6U CubeSat Design Specifications”, URL: http://www.cubesat.org/ [retrieved 25 June 2018]
[28] Morsch Filho, E.; Bohrer, E.; Possamai, T.S.; Paiva, K. V.; Travassos Junior, X. L., “Numerical investigation of the influence of the orbit inclination on thermal control of a nanosatellite in LEO”, II Latin American IAA CubeSat Workshop, 2016, Florianopolis.